Nonlinear Observer Based on Linear Matrix Inequalities for Sensorless Grid-tied Single-stage Photovoltaic System

Raul Antonio de Jesus TERAN-GONZALEZ, Javier PEREZ, Jose Antonio BERISTAIN
Technological Institute of Sonora, Electrical and Electronics Department, 85137, Mexico
javier.perezr@itson.edu.mx

***Abstract*—The objective of this work is to design a Nonlinear Observer used in a Cascade Control scheme for Maximum Power Point Tracking goals of a grid-tied single-phase photovoltaic inverter. The main contribution of this work is to employ a nonlinear observer to reduce the number of sensors of an AC-grid-tied single-stage PV system. The nonlinear observer design was developed using the Takagi-Sugeno PV system model and Linear Matrix Inequalities based on Lyapunov stability criteria. To validate the performance of the nonlinear observer-based cascade control, the results of a comparison between the PV system with observer (without DC voltage sensor) and a PV system with DC voltage sensor (without observer) are presented. A suitable PV power estimation with the nonlinear observer-based cascade control is achieved, which allowing a good performance of the MPPT algorithms. Perturb & Observe and Incremental Conductance MPPT algorithms were used.**

***Index Terms*—DC-AC power converters, maximum power point trackers, linear matrix inequalities, observers, takagi-Sugeno model.**

I. INTRODUCTION

The photovoltaic (PV) system classification can be divided into isolated and grid-tied systems [1]. Isolated PV systems require an energy storage system, which is suitable for low power systems. On the other hand, grid-tied PV systems do not require an energy storage system, and they have become the main PV application in high power systems [2-4]. Grid-tied PV systems aim to improve the efficiency and reliability in every PV system stage [4], and inject the maximum power from the PV array to the electrical grid. To extract the maximum PV power (P_{mp}), PV module features must be considered. Voltage and current in the PV array change in a nonlinear form when a variation in temperature or irradiation is presented, then the optimum operating point of the PV array for the maximum PV power, also known as Maximum Power Point (MPP), is modified [5]. Once the maximum power voltage (V_{mp}) is established in the PV array terminals then the maximum power current (I_{mp}) is obtained, and vice versa. In this way, for each temperature and irradiation condition, the Maximum Power Point Tracking (MPPT) consists of finding either the V_{mp} or I_{mp} corresponding to the MPP of the PV array. In order to operate a PV system in the MPP, several MPPT algorithms have been reported in the literature [5], such as Fractional Open-Circuit Voltage [6], Fractional Short-Circuit Current [7], Hill Climbing [8], Perturb & Observe (P&O) [9], Incremental Conductance (IC) [10], among others, as well as hybrid MPPT schemes [11-12].

Grid-tied PV systems can be divided into single-stage and two-stage PV systems [1], [13-14]. A single-stage PV system only consists of a DC-AC converter to carry out the MPPT as well as transferring the maximum PV power to the mains. On the other hand, a two-stage PV system is composed of two cascade converters [2], [15-16], the first one is a DC-DC converter fully dedicated to developing the MPPT, whereas the second one is a DC-AC converter used to transfer the maximum PV power to the mains. This two-stage scheme is the most widely used in PV systems, as a consequence a great number of works of MPPT for DC-DC converters in two-stage PV systems have been reported [17-19]. Although it is easier to implement the MPPT algorithm in a two-stage PV system, this last one represents a bulky and less efficient system [20]. The maximum PV power extraction essentially depends on the power converter efficiency and the MPPT algorithm effectiveness; thus, a way to improve the PV system efficiency is putting away the DC-DC stage, only keeping the inverter stage between the PV array and the mains. This single-stage PV system allows operating with a compact and less expensive system [3-4], [20]. This paper approaches grid-tied single-stage PV systems and the most employed MPPT algorithms such as P&O and IC.

To develop the MPPT, PV array voltage and current signals are required. One way to obtain these signals is through the use of DC voltage and current sensors [13], [21], which implementation cost needs to be covered; besides, using sensors could cause noise in the control scheme. Alternatively, employing observer schemes is possible, which make use of the input and output of the system to estimate state variables [22]. To carry out the sensorless MPPT task and considering the PV power nonlinear dynamics, a nonlinear observer is suitable.

Some sensor reduction strategies in grid-tied single-stage PV systems are presented in the following works. A cascade H-Bridge multilevel converter-based PV system with no voltage or current sensors at the DC-side is proposed in [23], where one advantage is the reduced number of sensors for a three-cell multilevel topology; this work only uses AC-side sensors, however, these AC sensors induce noise, which is harder to mitigate, in comparison with DC sensors, and the noise could significantly affect the control signal. In [24], a grid-tied PV-inverter control strategy is used to carry out an

This work was supported by CONACYT doctorate scholarship 768792 and the funds provided by the PROFAPI and PROFEXCE programs from ITSON.

Digital Object Identifier 10.4316/AECE.2021.03011

MPPT with no sensors at the DC-side. In this work, the P&O algorithm was used. The perturbed signal oscillations, corresponding to the converter output AC-power, are reduced; however, the MPP convergency time is much greater than in the case of an MPPT version with DC-side current and voltage sensors. In [25] a controller with an estimator is employed. This allows to discard the PV array current sensor in an MPPT based on the direct-gradient descent method; although the number of the DC-side sensors is reduced, the design criteria do not consider the converter power losses, which can lead to uncertainty in the MPP estimation.

In contrast with previously described works, Linear Matrix Inequalities (LMI) and the Takagi-Sugeno (TS) models are used in this work to design a nonlinear observer. Although LMIs and TS are designing tools mainly employed in mechanic and mechatronic systems, their use in the nonlinear observer design for a grid-tied single-stage PV system is shown in this work. Also, MPPT algorithms such as P&O and IC are used. The observer design through the use of exact TS models has recently taken a great interest [26], this is because of the TS models allow obtaining an exact representation of a great family of nonlinear models, through the use of sector nonlinearity approach [27]. This methodology is adequate for the exact nonlinear representation of the PV array and power converter nonlinear dynamics of this work. In this way, this system representation corresponds to a convex structure which captures the nonlinearities of the original PV system model, and from that, it allows to establish an LMI form conditions which can be solved by convex optimization methods [28]. Thus, the TS-LMI-based nonlinear observer allows estimating the desired signal, which in this case is the DC-side voltage, which asymptotically approximates the real signal allowing a good MPP estimation.

In order to carry out the MPPT without employing a DC voltage sensor in the PV array terminals, the objective of this work is to design a nonlinear observer employed in a cascade control scheme for a grid-tied single-stage PV system. The Nonlinear Observer-Based Cascade Control (NOBCC) includes: (a) a nonlinear observer to estimate the DC voltage in the PV array terminals, which design is carried out using the system exact TS model and solving the Lyapunov-based LMI conditions [28]; (b) a cascade control scheme composed by two control loops, an outer control loop with a PI controller for the DC voltage regulation, and an inner control loop with a PI controller for the reference current tracking; (c) P&O and IC MPPT algorithms which are fed with an observed DC voltage and an estimated PV power. The main contribution of this work is to use a TS-LMI-based nonlinear observer in order to put away the DC voltage sensor used at the PV array terminals for MPPT tasks.

The organization of this article is described as follows. The description and modeling of the grid-tied single-stage PV system is presented in section II. In section III, the nonlinear observer design is shown. The complete NOBCC scheme is described in section IV. Simulation results are exposed in section V; and finally, conclusions are given in section VI.

II. Description and PV System Modeling

In Fig. 1 the PV system of this work is shown, which is composed of a DC-AC converter. DC-side includes a PV array, a capacitor C, and a resistance R. This R represents the active power losses of the DC bus. AC-side includes an inductor L, which smooths the abrupt changes in the output current i_L, allowing the coupling with the mains. Besides, the involved sensors in the system are those which provide the following signals: PV array current i_{pv}, inductor current i_L, and the grid voltage v_g. It is important to clarify that, the PV system has not a sensor for the DC voltage v_C; thus, v_C will be estimated by the nonlinear observer. The DC-AC converter corresponds to a single-phase H-Bridge composed of four MOSFET ($T_{1,2,3,4}$) with anti-parallel diodes ($D_{1,2,3,4}$), which together allow bidirectional power transfer. The MOSFET is activated by a Sinusoidal Pulse Width Modulation (SPWM) strategy, in which switching frequency is denoted as f_s. The passive elements sizing and the system operating parameters are presented in Table I. The PV array was designed considering the serial connection of 17 solar modules (30W Monocrystalline silicon TUV/CE PV Solar cells-DBF30) with a maximum power of 30 W each one, obtaining a total power capacity of 511.7 W with $V_{mp} = 297.5$ V and $I_{mp} = 1.72$ A, at 25 °C and 1 kW/m^2.

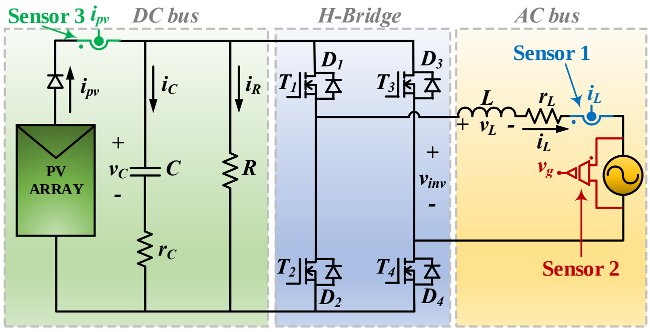

Figure 1. Scheme of the grid-tied single-stage PV system

TABLE I. Description of the PV System Parameters

Parameter	Description	Value
C	DC-link capacitor	1 mF
r_C	Parasite resistance of C	0.1 Ω
R	Loss resistance	1 kΩ
L	Coupling inductor	7 mH
r_L	Parasite resistance of L	0.18 Ω
v_g	Electrical grid voltage	127 V_{rms}
v_{inv}	Inverter output voltage	-
v_L	Coupling inductor voltage	-
i_C	DC-Bus capacitor current	-
i_R	Converter losses current	-
f_s	Switching frequency	12 kHz

There are several techniques for modeling switched power systems, one of them is the use of the extended harmonic domain models; recent improved versions are reported in [29].

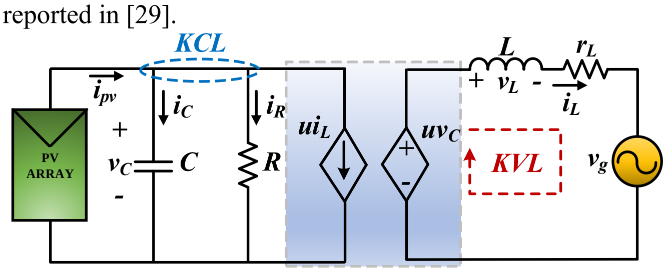

Figure 2. Equivalent scheme of grid-tied single-phase PV system

However, this work makes use of an averaged fundamental frequency model to represent the PV system dynamics. To obtain the PV system model, in Fig. 2 an equivalent PV system is presented, where the H-Bridge is replaced by current and voltage controlled sources.

Since i_L is the state variable, the Kirchhoff voltage law (KVL) is applied in the AC bus mesh of Fig. 2, obtaining:

$$L\frac{di_L}{dt} = uv_C - r_L i_L - v_g \tag{1}$$

Knowing that v_C is the second state variable and applying the Kirchhoff current law (KCL) in the DC bus node of Fig. 2 then:

$$C\frac{dv_C}{dt} = i_{pv} - ui_L - \frac{v_C}{R} \tag{2}$$

Considering $x_1 = i_L$ and $x_2 = v_C$, the PV system model is:

$$L\dot{x}_1 = ux_2 - r_L x_1 - v_g \tag{3}$$

$$C\dot{x}_2 = i_{pv} - ux_1 - \frac{x_2}{R} \tag{4}$$

In this way, (3) and (4) make up the PV system averaged model, where u is the control signal given by:

$$u = m\cos(\omega t + \alpha) \tag{5}$$

where m is the signal amplitude, $\omega = 2\pi 60$, α is the phase angle with respect to v_g, and t is the time. The next section shows the nonlinear observer design, which largely depends on u.

III. Nonlinear Observer Design

To estimate the DC voltage v_C in the PV array terminals, a nonlinear observer is required. For this particular design, the measured signals i_L and the control law u are considered, which are the input and output of the system, respectively. From the averaged model given in (3) and (4), the nonlinear PV system is:

$$\underbrace{\begin{bmatrix}\dot{x}_1\\ \dot{x}_2\end{bmatrix}}_{\dot{\mathbf{x}}} = \underbrace{\begin{bmatrix}-\frac{r_L}{L} & \frac{u}{L}\\ -\frac{u}{C} & -\frac{1}{RC}\end{bmatrix}}_{\mathbf{A}}\underbrace{\begin{bmatrix}x_1\\ x_2\end{bmatrix}}_{\mathbf{x}} + \underbrace{\begin{bmatrix}-\frac{v_g}{L}\\ \frac{i_{pv}}{C}\end{bmatrix}}_{\mathbf{W}},\ y = \underbrace{\begin{bmatrix}1 & 0\end{bmatrix}}_{\mathbf{C}}\mathbf{x} \tag{6}$$

which can be seen as:

$$\begin{gathered}\dot{\mathbf{x}}(t) = \mathbf{A}(u)\mathbf{x}(t) + \mathbf{W}(v_g, i_{pv})\\ y(t) = \mathbf{C}\mathbf{x}(t)\end{gathered} \tag{7}$$

where $\mathbf{x}(t) \in \mathbb{R}^2$, $\mathbf{W}(v_g, i_{pv}) \in \mathbb{R}^2$ and the output $y(t) \in \mathbb{R}$; besides, $\mathbf{A}$ and $\mathbf{C}$ are matrices of suitable dimensions, and $\mathbf{x}(t) = [x_1 \quad x_2]^T$ is the state variable vector of the original system. Considering (7) and based on [30], the used nonlinear observer has the following form:

$$\begin{gathered}\dot{\hat{\mathbf{x}}}(t) = \mathbf{A}(u)\hat{\mathbf{x}}(t) + \mathbf{W}(v_g, i_{pv}) + \mathbf{L}_\delta\left(y(t) - \hat{y}(t)\right)\\ \hat{y}(t) = \mathbf{C}\hat{\mathbf{x}}(t)\end{gathered} \tag{8}$$

where $\mathbf{A}$, $\mathbf{W}$ and $\mathbf{C}$ are the matrices shown in (6), and $\hat{\mathbf{x}}(t) = [\hat{x}_1 \quad \hat{x}_2]^T$ is the state variable vector of the nonlinear observer; the nonlinear gain $\mathbf{L}_\delta$ is given as in (9), where $\mathbf{L}_j$, $j = 1,2,...,r$ with $r = 2^q$ (q denotes the number of nonconstant signals which are associated with nonlinearities in the system model) is each of the linear gain vectors, which are obtained by solving the LMI feasibility problem. Likewise, terms $h_j(z)$ correspond to membership functions which will be defined later.

$$\mathbf{L}_\delta = \sum_{j=1}^{r} h_j(z)\mathbf{L}_j \tag{9}$$

To synthesize $\mathbf{L}_\delta$, the system nonlinearities must be identified. The products ux_2 and ux_1 seen in (3) and (4), respectively, correspond to the PV system nonlinearities; thus, the control signal u is the only nonconstant signal in **A**, which is associated with nonlinearities in the PV system, thus $q = 1$. Now, using the sector nonlinearity approach [27], [30], a premise vector $\mathbf{z}(\cdot)$ that contains the nonconstant terms z_k, $k = 1,2,...,q$, has to be used; in this way, the vector $\mathbf{z}$ only includes one term denoted as $z_1 = u$. The signal u in $\mathbf{z}$ will be bounded in a predefined compact set $\Omega \subseteq \mathbb{R}$ with $z_1^0 \le z_1(u) \le z_1^1$, where z_1^0 and z_1^1 correspond to the minimum and maximum value of $z_1(u)$ in Ω, respectively. Due to the SPWM requirements, the control signal is bounded as:

$$u \in [-1, 1] \tag{10}$$

Considering $z_1(u) \in [z_1^0, z_1^1]$, $z_1(u)$ can be rewritten as a convex sum of its bounds, this is:

$$z_1(u) = \omega_0^1(u) z_1^0(u) + \omega_1^1(u) z_1^1(u) = \sum_{i_1=0}^{1} \omega_{i_1}^1(u) z_1^{i_1} \tag{11}$$

where:

$$\omega_0^k(u) = \frac{z_1^1 - z_1(u)}{z_1^1 - z_1^0},\quad \omega_1^1(u) = 1 - \omega_0^1(u) \tag{12}$$

Terms ω_0^1 and ω_1^1 in (12) are known as weights, which comply with the convex sum property given by:

$$\omega_0^1(u) + \omega_1^1(u) = 1,\ \omega_0^1(u), \omega_1^1(u) \in [0,1] \tag{13}$$

in the compact Ω [26]. Now, taking into account the bounds in (10) and the weights in (12) then:

$$\omega_0^1(z_1) = \frac{1 - z_1(u)}{2},\quad \omega_1^1(z_1) = \frac{1 + z_1(u)}{2} \tag{14}$$

Now, membership functions are defined as follows:

$$h_i(z_1(u)) = \prod_{j=1}^{q} \omega_{i_j}^1(z_1(u)),\ i = 1,2,...,2^q \tag{15}$$

In this particular design, only one nonconstant term is considered, thus membership functions are:

$$h_1 = \omega_0^1(z_1),\quad h_2 = \omega_1^1(z_1) \tag{16}$$

Now, considering the modeling region Ω, the exact convex rewriting of the system (6) is:

$$\dot{\mathbf{x}} = \sum_{i=1}^{2} h_i(z_1(u))\mathbf{A}_i\mathbf{x} + \mathbf{W},\ y = \sum_{i=1}^{2} h_i(z_1(u))\mathbf{C}_i\mathbf{x} \tag{17}$$

where $\mathbf{W}$ as shown in (6), and matrices $\mathbf{A}_i$ and $\mathbf{C}_i$ are linear matrices which are obtained as follows. Firstly, $\mathbf{A}_1$ is obtained by substituting u by its minimum bound $(z_1^0 = -1)$ in matrix **A** when $h_1 = 1$, and $\mathbf{A}_2$ is obtained by substituting u by its maximum bound $(z_1^1 = 1)$ in **A** when

$h_2 = 1$. Only linear terms are contained in the output vector, then $\mathbf{C}_1$ and $\mathbf{C}_2$ are equal to $\mathbf{C}$. These linear matrices are shown in (18) and they allow to form local TS models.

$$\mathbf{A}_1 = \begin{bmatrix} -\frac{r_L}{L} & -\frac{1}{L} \\ \frac{1}{C} & -\frac{1}{RC} \end{bmatrix}, \mathbf{A}_2 = \begin{bmatrix} -\frac{r_L}{L} & \frac{1}{L} \\ -\frac{1}{C} & -\frac{1}{RC} \end{bmatrix}, \quad \mathbf{C}_1 = \begin{bmatrix} 1 & 0 \end{bmatrix}, \quad \mathbf{C}_2 = \begin{bmatrix} 1 & 0 \end{bmatrix} \tag{18}$$

To design the nonlinear observer, local TS models must be observable [30-31]. The nonlinear observer for (17) is:

$$\dot{\hat{\mathbf{x}}} = \sum_{i=1}^{2}\sum_{j=1}^{2} h_i(u)h_j(u)\left(\mathbf{A}_i\hat{\mathbf{x}} - \mathbf{L}_j\mathbf{C}_i(\mathbf{x}-\hat{\mathbf{x}})\right) + \mathbf{W} \tag{19}$$

From the estimation error $\mathbf{e}(t) = \mathbf{x}(t) - \hat{\mathbf{x}}(t)$ then $\dot{\mathbf{e}}(t) = \dot{\mathbf{x}}(t) - \dot{\hat{\mathbf{x}}}(t)$ is:

$$\dot{\mathbf{e}}(t) = \sum_{i=1}^{2}\sum_{j=1}^{2} h_i(u)h_j(u)(\mathbf{A}_i - \mathbf{L}_j\mathbf{C}_i)\mathbf{e}(t) \tag{20}$$

Considering the dynamics in (20), a Lyapunov quadratic function $V(\mathbf{e}(t)) = \mathbf{e}(t)^T \mathbf{P}\mathbf{e}(t)$ is used, then:

$$\dot{V} = \mathbf{e}^T\mathbf{P}\dot{\mathbf{e}} + \dot{\mathbf{e}}^T\mathbf{P}\mathbf{e} < 0 \tag{21}$$

Substituting (20) in (21), the obtained expression is:

$$\dot{V} = \sum_{i=1}^{2}\sum_{j=1}^{2} h_i h_j \mathbf{e}^T \underbrace{\left(\mathbf{P}\mathbf{A}_i + \mathbf{A}_i^T\mathbf{P} - \mathbf{P}\mathbf{L}_j\mathbf{C}_i - \mathbf{C}_i^T\mathbf{L}_j^T\mathbf{P}\right)}_{\gamma}\mathbf{e} \tag{22}$$

with $i, j = 1, 2, ..., r$. To obtain $\dot{V} < 0$ then $\gamma < 0$ must be satisfied, this is:

$$\mathbf{P}\mathbf{A}_i + \mathbf{A}_i^T\mathbf{P} - \mathbf{P}\mathbf{L}_j\mathbf{C}_i - \mathbf{C}_i^T\mathbf{L}_j^T\mathbf{P} < 0 \tag{23}$$

Notice that the expression in (23) is not an LMI condition yet, thus, to have only one decision variable in each term of (23) then a change variable $\mathbf{N}_j = \mathbf{P}\mathbf{L}_j$ is carried out. Now, $\hat{\mathbf{x}}(t)$ of the nonlinear state observer in (19) asymptotically approaches towards $\mathbf{x}(t)$ of the nonlinear original system in (17) if there are matrices $\mathbf{P} = \mathbf{P}^T > 0$ and $\mathbf{N}_j$, $j = 1, 2, ..., r$ with $r = 2^q$, such that LMI expression given as:

$$\mathbf{P}\mathbf{A}_i + \mathbf{A}_i^T\mathbf{P} - \mathbf{N}_j\mathbf{C}_i - \mathbf{C}_i^T\mathbf{N}_j^T < 0 \tag{24}$$

is satisfied, where the linear gain vectors of the observer are given by $\mathbf{L}_j = \mathbf{P}^{-1}\mathbf{N}_j$, $j = 1, 2, ..., r$. Thus, considering the system parameters exposed in Table I and using MATLAB LMIToolbox, LMI conditions in (24) are solved; thus, the linear gain vectors are:

$$\mathbf{L}_1 = \begin{bmatrix} \text{-25.2143} \\ 742.8571 \end{bmatrix}, \mathbf{L}_2 = \begin{bmatrix} \text{-25.2143} \\ \text{-742.8571} \end{bmatrix} \tag{25}$$

with $\mathbf{P} = \begin{bmatrix} 114.2586 & 0 \\ 0 & 63.4770 \end{bmatrix}$. Using gain vectors in (25) and the membership functions in (16), synthesizing the observer nonlinear gain in (9) is possible.

IV. NOBCC Scheme for P&O and IC MPPT Algorithms

This section describes the NOBCC scheme for the PV system and gives a description of the used MPPT algorithms. The NOBCC scheme for MPPT objectives, which includes a cascade control scheme and the nonlinear observer previously designed in section III, is shown in Fig. 3.

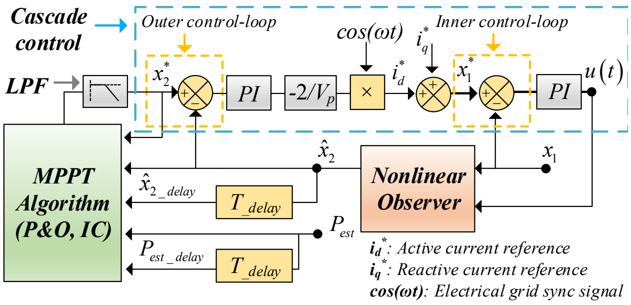

Figure 3. NOBCC scheme for MPPT goals

The cascade control is composed of an inner control loop to track the reference current and an outer control loop to regulate the estimated DC voltage [1], [14]. The current control consists of an inner control loop, which allows the PV system to transfer active power from the DC bus to the AC bus. Proportional-Integral (PI) controllers, in both outer and inner control loops, are used, and they are tuned based on [32]. The nonlinear observer receives the input and output PV system, which correspond to the control signal u and the inductor current x_1, respectively, as shown in Fig. 3. The observed DC voltage is denoted as $\hat{x}_2$ and is used as a feedback signal in the outer control loop to regulate the DC voltage. Now, to have a slower dynamic of the MPPT, a low pass filter (LPF) in the MPPT output is added; this output corresponds to the reference voltage x_2^*; in this way, $\hat{x}_2$ can track x_2^*.

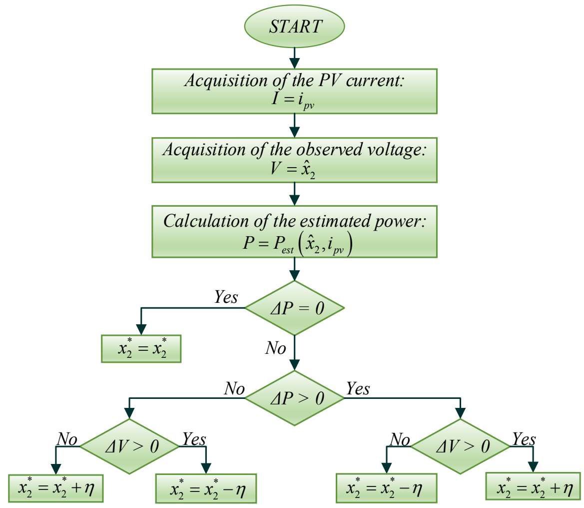

Figure 4. P&O algorithm flowchart with estimated and observed signals

To extract the maximum power from the PV array, the P&O and IC MPPT algorithms are employed; the MPPT is carried out using an iteration time denoted as T_{delay}. The MPPT block (Fig. 3) uses two pairs of signals as input; the first pair corresponds to the present observed DC voltage $\hat{x}_2$ and the observed DC voltage delayed at T_{delay}, which is denoted as $\hat{x}_{2\_delay}$; the second pair corresponds to the estimated PV power P_{est} and its delayed version P_{est_delay}, where P_{est} is given by (26).

$$P_{est} = \hat{x}_2 \cdot i_{pv} \tag{26}$$

A positive constant η is added to increase or decrease the value of x_2^* during the search of V_{mp}. Fig. 4 shows the P&O algorithm flowchart [33], which calculates the voltage and power changes as follows:

$$\Delta V = \hat{x}_2 - \hat{x}_{2\_delay} \tag{27}$$

$$\Delta P = P_{est} - P_{est\_delay} \tag{28}$$

The P&O algorithm generally operates perturbing (increasing or decreasing) the operating voltage and observing the power dynamics ΔP; in this way, changes in x_2^* (ΔV) to reach the MPP are realized [21]. Due to the good performance of the nonlinear observer to estimate ΔP correctly, the P&O algorithm can offer a reference voltage close to V_{mp}. The IC algorithm flowchart [33] is shown in Fig. 5. Unlike P&O, IC operates with $\hat{x}_2$ and i_{pv}, where this last one is obtained by (29), and its delayed version is given in (30).

$$i_{pv} = \frac{P_{est}}{\hat{x}_2} \tag{29}$$

$$i_{pv\_delay} = \frac{P_{est\_delay}}{\hat{x}_{2\_delay}} \tag{30}$$

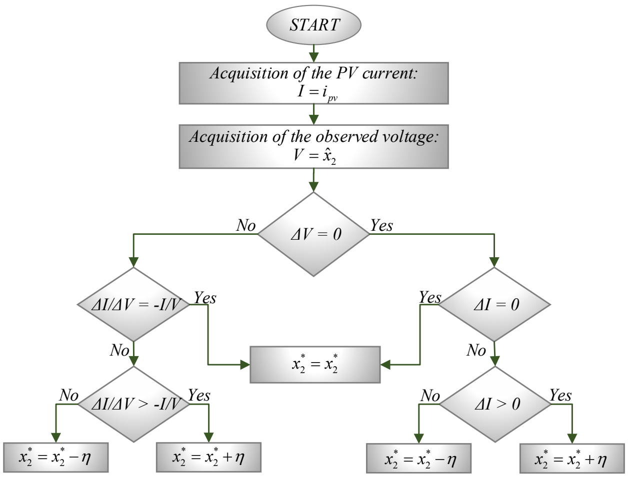

Figure 5. IC algorithm flowchart with estimated and observed signals

Besides ΔV, the IC algorithm uses the PV current change, ΔI, which is obtained as:

$$\Delta I = i_{pv} - i_{pv\_delay} \tag{31}$$

The IC algorithm is based on the fact that the curve slope of the PV power is equal to zero at the MPP, positive at the left of MPP, and negative at the right [5]. PV power derivative respect the voltage is:

$$\frac{dP}{dV} = \frac{d(VI)}{dV} = I + V\frac{dI}{dV} \approx I + V\frac{\Delta I}{\Delta V} = \frac{\Delta P}{\Delta V} \tag{32}$$

where incremental conductance is denoted as $\Delta I/\Delta V$, and the dynamic of the slope $\Delta P/\Delta V$ changes in function of the value that takes $\Delta I/\Delta V$ with respect to the instantaneous conductance, which is denoted as I/V. Considering the previous description, the PV power slope can be defined by (33). Therefore, IC algorithm modifies the voltage operating point considering the state of the PV power slope. In this way, the output, in both P&O and IC algorithms, is the reference voltage x_2^* (Fig. 3), which has to reach V_{mp}.

$$\begin{cases} I + V(\Delta I/\Delta V) = 0 & if \quad \Delta I/\Delta V = -I/V \\ I + V(\Delta I/\Delta V) > 0 & if \quad \Delta I/\Delta V > -I/V \\ I + V(\Delta I/\Delta V) < 0 & if \quad \Delta I/\Delta V < -I/V \end{cases} \tag{33}$$

The success of the extraction of the maximum PV power depends on the joint work of MPPT algorithms and NOBCC scheme.

V. Simulation Tests and Discussion of Results

Using PSIM® environment, the PV system circuit and the SPWM scheme, seen in Fig. 1, were implemented; system parameters, from Table I, were employed. For programing the NOBCC scheme, MATLAB/Simulink was used. Fig. 6 shows the stages of the NOBCC scheme implemented in Simulink, such as the cascade control scheme, the nonlinear observer, and the MPPT algorithm; also, to synchronize the converter to the mains, a Phase Locked Loop (PLL) was used. To maintain a communication link with the PSIM® circuit, a SimCoupler module was employed. Through the SimCoupler module was possible to send the control signal u to the SPWM scheme; also, both the irradiation and temperature levels were sent to PSIM® for changing the MPP in the PV array. Likewise, the sensed signals i_L, v_g, and i_{pv} were received from PSIM® toward Simulink.

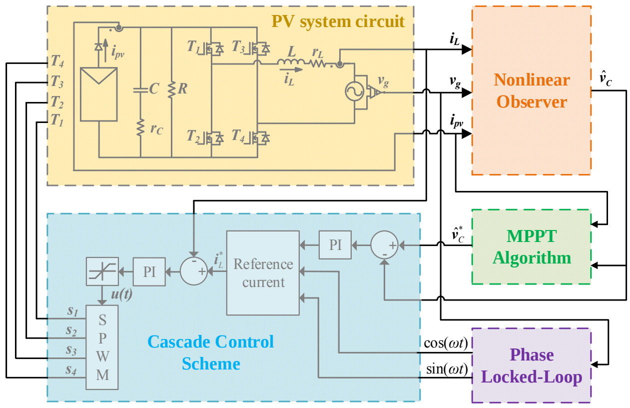

Figure 6. General diagram for NOBCC implementation

TABLE II. IRRADIATION AND TEMPERATURE TEST CONDITIONS

Irradiation (W/m²)	Temperature (°C)	Hour
100	28.3	8:50
400	31.5	10:20
800	36.4	12:30
1000	37.9	14:20
700	40.8	17:20
500	40.4	18:20
300	40	19:10

For the operation of MPPT algorithms, the parameters $T_{delay} = 10\mu s$ and $\eta = 1$ were used. Proportional gain $k_{P1} = 0.029$ and an integral gain $k_{I1} = 502.4836$ in the inner control loop were used, whereas, for the outer control loop, proportional gain $k_{P2} = 10.5348$ and integral gain $k_{I2} = 66.1922$ were used [32]. Simulation tests are based on solar irradiation and temperature changes, as seen in Table II; these data correspond to the coordinates: latitude 29.07833 and length -110.93027, in which Hermosillo city from Sonora state in Mexico is located.

A. NOBCC Performance for DC Voltage Regulation

Before presenting NOBCC results for MPPT conditions, a NOBCC performance validation for changes in the DC voltage reference is illustrated. Fig. 7 shows the regulation and DC voltage estimation through the NOBCC scheme; notice in Fig. 7 that, for each voltage reference change, a very similar behavior between the estimated voltage $\hat{x}_2$ and the measured DC voltage x_2 is kept. This result highlights the good capacity of the observer for estimating the DC voltage.

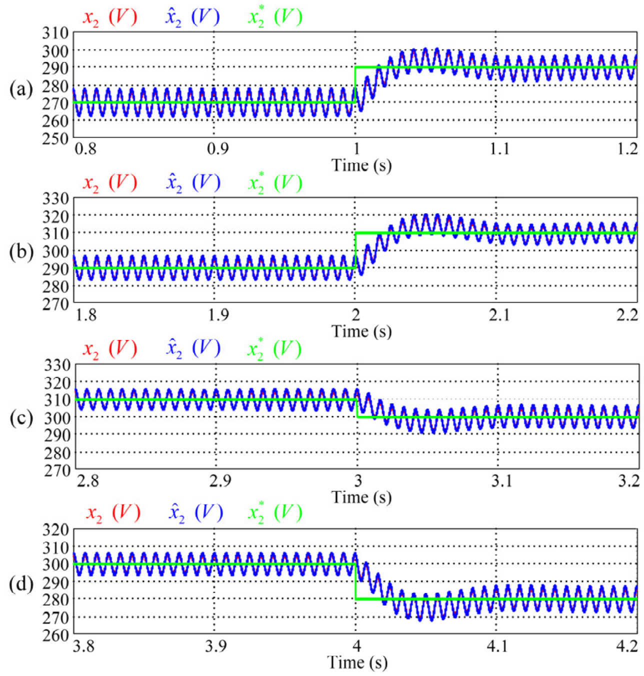

Figure 7. Regulation and DC voltage estimation with NOBCC scheme: (a) from $x_2^* = 270\ V$ to $x_2^* = 290\ V$, (b) from $x_2^* = 290\ V$ to $x_2^* = 310\ V$, (c) from $x_2^* = 310\ V$ to $x_2^* = 300\ V$, (d) from $x_2^* = 300\ V$ to $x_2^* = 280\ V$.

B. NOBCC Performance with P&O MPPT Algorithm

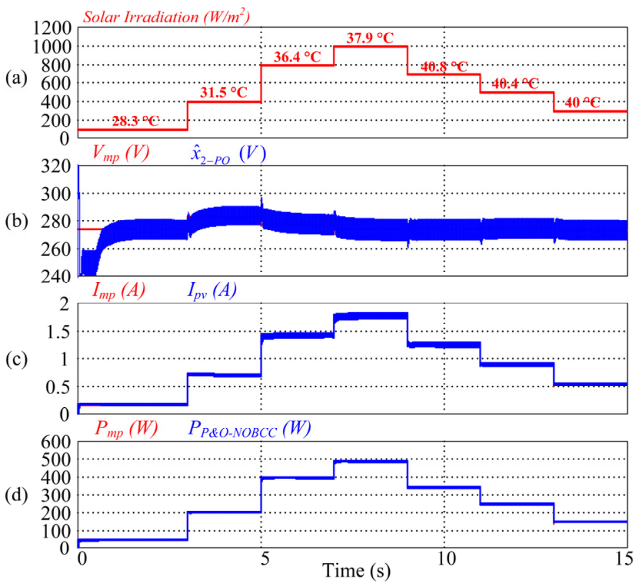

Figure 8. Results of the NOBCC with P&O algorithm for MPPT goals: (a) irradiation and temperature values; (b) tracking of the maximum power voltage V_{mp}; (c) tracking of the maximum power current Imp; (d) maximum PV power extraction P_{mp}

Fig. 8 shows NOBCC results for the MPPT task with the P&O algorithm. All irradiation and temperature levels are observed in plot (a) from Fig. 8. As seen in plot (b), due to the good performance of the nonlinear observer and P&O algorithm, the observed voltage $\hat{x}_{2-PO}$ remains around V_{mp} in each irradiation and temperature level. As a consequence, i_{pv} values overlapping with the I_{mp} levels in each irradiation and temperature level, as seen in plot (c). Finally, in plot (d) a correct tracking of the estimated PV power ($P_{P\&O\text{-}NOBCC}$) with respect to the maximum power (P_{mp}) available in the PV array is presented. In Table III a comparison between the obtained results of the NOBCC using P&O algorithm and the expected MPP values in each irradiation and temperature level is presented; note that expected and obtained results are similar.

TABLE III. RESULTS OF P&O MPPT ALGORITHM CORRESPONDING TO EACH SOLAR IRRADIATION AND TEMPERATURE LEVEL

Irrad. (W/m^2)	Temp. (°C)	P_{mp} (W)	$P_{P\&O\text{-}NOBCC}$ (W)	V_{mp} (V)	$\hat{x}_{2\text{-}PO}$ (V)	I_{mp} (A)	i_{pv} (A)
100	28.3	49.36	50.04	274.26	274.04	0.18	0.1826
400	31.5	204.19	205.04	283.60	283.06	0.72	0.7245
800	36.4	400.29	399.60	277.98	278.75	1.44	1.4340
1000	37.9	491.08	491.04	274.35	274.24	1.79	1.7911
700	40.8	345.79	346.59	274.44	274.01	1.26	1.2652
500	40.4	250.48	250.06	275.26	274.91	0.91	0.9098
300	40	150.38	151.01	273.43	273.77	0.55	0.5517

C. NOBCC Performance with IC MPPT Algorithm

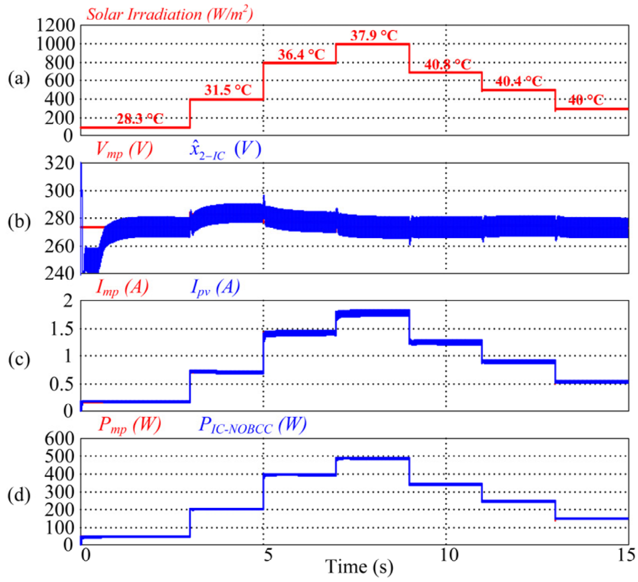

Figure 9. Results of the NOBCC with IC algorithm for MPPT goals: (a) irradiation and temperature values; (b) tracking of the maximum power voltage V_{mp}; (c) tracking of the maximum power current Imp; (d) maximum PV power extraction P_{mp}

In the same way, as with the P&O algorithm case, plot (a) in Fig. 9 presents the same solar irradiation and temperature levels, which are considered for the PV system. Plot (b) shows the behavior of $\hat{x}_2$ for the MPPT with IC ($\hat{x}_{2-IC}$), note that $\hat{x}_{2-IC}$ remains in the vicinity of V_{mp} for each irradiation and temperature level, then i_{pv} reaches the values of I_{mp}, as seen in plot (c). Thus, the performance of the IC algorithm with the NOBCC allows carrying out a good estimation of P_{mp}; in this case, this estimated power ($P_{IC\text{-}NOBCC}$) is remarkably similar to P_{mp}, as seen in plot (d).

Results of IC algorithm with NOBCC are compared with the expected results in Table IV; expected values are very close to the obtained values.

TABLE IV. RESULTS OF IC MPPT ALGORITHM CORRESPONDING TO EACH SOLAR IRRADIATION AND TEMPERATURE LEVEL

Irrad. (W/m^2)	Temp. (°C)	P_{mp} (W)	$P_{IC\text{-}NOBCC}$ (W)	V_{mp} (V)	$\hat{x}_{2-IC}$ (V)	I_{mp} (A)	i_{pv} (A)
100	28.3	49.36	50.04	274.26	274.05	0.18	0.1826
400	31.5	204.19	205.04	283.60	283.06	0.72	0.7245
800	36.4	400.29	399.60	277.98	278.75	1.44	1.4340
1000	37.9	491.08	491.04	274.35	274.24	1.79	1.7911
700	40.8	345.79	346.59	274.44	274.00	1.26	1.2653
500	40.4	250.48	250.06	275.26	274.91	0.91	0.9098
300	40	150.38	151.01	273.43	273.77	0.55	0.5517

D. Observer Performance vs Voltage Sensor Performance

Now, a comparison between the performance of the nonlinear observer and a DC voltage sensor in PV array terminals is carried out. It is important to clarify that these tests with the DC voltage sensor are carried out using the same cascade control scheme as NOBCC, but in this case, a voltage sensor is used instead of the nonlinear observer. Table V presents a summary of the estimated voltages by the observer, $\hat{x}_{2-PO}$ and $\hat{x}_{2-IC}$, which were included in Table III and Table IV, respectively; also, Table V includes the obtained voltage ($v_{mp\text{-}sensor}$) in the sensor tests.

TABLE V. OBSERVED VOLTAGES VS SENSED VOLTAGES

Irrad. (W/m^2)	Temp. (°C)	V_{mp} (V)	$v_{mp\text{-}sensor}$ (V)	$\hat{x}_{2-PO}$ (V)	$\hat{x}_{2-IC}$ (V)
100	28.3	274.26	274.40	274.04	274.05
400	31.5	283.60	283.53	283.06	283.06
800	36.4	277.98	278.16	278.75	278.75
1000	37.9	274.35	274.55	274.24	274.24
700	40.8	274.44	274.64	274.01	274.00
500	40.4	275.26	275.40	274.91	274.91
300	40	273.43	273.64	273.77	273.77

For each irradiation and temperature level, the voltage obtained by the sensor is very similar to the expected value for both MPPT algorithms, as seen in Table V. In the same way, the observed voltage for each irradiation and temperature level is very similar to the sensed voltage, with a marginal difference. This marginal difference does not represent a significant impact on the obtained total power, as seen in Fig. 10 and Fig. 11.

A comparison among the extracted powers using nonlinear observer and DC voltage sensor is presented in Fig. 10 and Fig. 11. Also, in both figures, the available maximum PV power P_{mp} is included. The obtained powers for the PV system using DC voltage sensor are denoted as $P_{P\&O\text{-}Sensor}$, Fig. 10, and $P_{IC\text{-}Sensor}$, Fig. 11, for P&O and IC algorithms, respectively. The results show a remarkable similarity between the extracted PV power using MPPT with NOBCC and the extracted PV power using MPPT with DC voltage sensor; in both cases, the MPP conditions are reached for each irradiation and temperature level.

In comparison with works such as [14], [24], the NOBCC scheme achieves a faster PV power estimation for both MPPT algorithms. Also, using the NOBCC scheme in single-stage PV systems, allows results as good as works where two-stage PV systems are used, such as [1], [13], [15-16], [34-35]. These facts allow the replacement of the DC voltage sensor by the nonlinear observer designed from the TS models and LMI conditions.

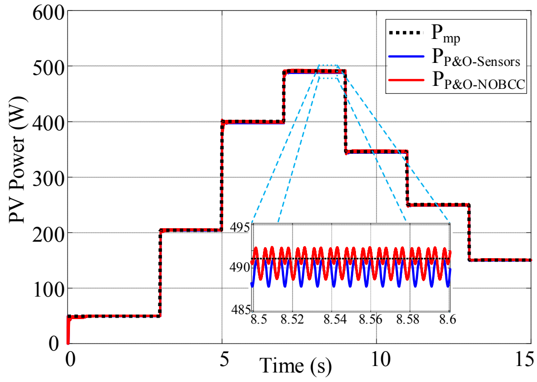

Figure 10. Comparative results between the P&O MPPT algorithm with observer and the P&O MPPT algorithm with sensor

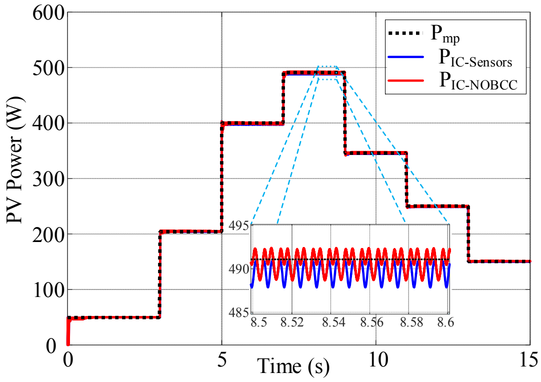

Figure 11. Comparative results between the IC MPPT algorithm with observer and the IC MPPT algorithm with sensor

VI. CONCLUSIONS

TS models and LMI conditions made possible to design a nonlinear observer to remove the DC voltage sensor in the PV array terminals for MPPT tasks. To guarantee the nonlinear observer performance in a grid-tied single-stage PV system, a cascade control scheme was required; thus, the nonlinear observer in conjunction with a cascade control was implemented, resulting in a nonlinear observer-based cascade control denoted as NOBCC. The nonlinear observer effectiveness in the NOBCC scheme was validated through a comparison against the cascade control scheme with the DC voltage sensor; similar results in the dynamics of the PV power extraction in both cases were obtained. P&O and IC MPPT algorithms were used in this comparison. A fast convergence during the PV power estimation for both MPPT algorithms was achieved by the NOBCC scheme; this fact allowed validating the replacement of the DC voltage sensor by the nonlinear observer designed from the TS models and LMI conditions.

REFERENCES

[1] V. Kumar and M. Singh, “Sensorless DC-link control approach for three-phase grid integrated PV system,” International Journal of Electrical Power & Energy Systems, vol. 112, pp. 309–318, Nov. 2019. doi:10.1016/j.ijepes.2019.05.006

[2] M. Guisser, E. Abdelmounim, M. Aboulfatah, and A. EL-Jouni, “Nonlinear observer-based control for grid connected photovoltaic system,” IOSR Journal of Electrical and Electronics Engineering, vol. 9, pp. 40–52, Jan. 2014. doi:10.9790/1676-09524052

[3] M. El malah, A. Ba-Razzouk, M. Guisser, E. Abdelmounim, M. Madark, and H. Bahri, “Nonlinear control for three phase single stage grid connected PV system,” in 2018 Renewable Energies, Power Systems Green Inclusive Economy (REPS-GIE), Apr. 2018, pp. 1–6. doi:10.1109/REPSGIE.2018.8488784

[4] V. N. Lal and S. N. Singh, "Control and performance analysis of a single-stage utility-scale Grid-connected PV system," IEEE Systems Journal, vol. 11, no. 3, pp. 1601–1611, Sep. 2017. doi:10.1109/JSYST.2015.2408055

[5] B. Subudhi and R. Pradhan, "A comparative study on maximum power point tracking techniques for photovoltaic power systems," IEEE Transactions on Sustainable Energy, vol. 4, no. 1, pp. 89–98, Jan. 2013. doi:10.1109/TSTE.2012.2202294

[6] M. M. Shebani, T. Iqbal, and J. E. Quaicoe, "Comparing bisection numerical algorithm with fractional short circuit current and open circuit voltage methods for MPPT photovoltaic systems," in 2016 IEEE Electrical Power and Energy Conference (EPEC), Oct. 2016, pp. 1–5. doi:10.1109/EPEC.2016.7771689

[7] H. A. Sher, A. F. Murtaza, A. Noman, K. E. Addoweesh, and M. Chiaberge, "An intelligent control strategy of fractional short circuit current maximum power point tracking technique for photovoltaic applications," Journal of Renewable and Sustainable Energy, vol. 7, no. 1, p. 013114, Jan. 2015. doi:10.1063/1.4906982

[8] M. I. Bahari, P. Tarassodi, Y. M. Naeini, A. K. Khalilabad, and P. Shirazi, "Modeling and simulation of hill climbing MPPT algorithm for photovoltaic application," in 2016 International Symposium on Power Electronics, Electrical Drives, Automation and Motion (SPEEDAM), Jun. 2016, pp. 1041–1044. doi:10.1109/SPEEDAM.2016.7525990

[9] M. Killi and S. Samanta, "Modified perturb and observe MPPT algorithm for drift avoidance in photovoltaic systems," IEEE Transactions on Industrial Electronics, vol. 62, no. 9, pp. 5549–5559, Sep. 2015. doi:10.1109/TIE.2015.2407854

[10] R. I. Putri, S. Wibowo, and M. Rifa'i, "Maximum power point tracking for photovoltaic using incremental conductance method," Energy Procedia, vol. 68, pp. 22–30, Apr. 2015. doi:10.1016/j.egypro.2015.03.228

[11] S. Mohanty, B. Subudhi, and P. K. Ray, "A grey wolf-assisted perturb & observe MPPT algorithm for a PV system," IEEE Transactions on Energy Conversion, vol. 32, no. 1, pp. 340–347, Mar. 2017. doi:10.1109/TEC.2016.2633722

[12] A. Thangavelu, S. Vairakannu, and P. Deiva Sundari, "Linear open circuit voltage-variable step-size-incremental conductance strategy-based hybrid MPPT controller for remote power applications," IET Power Electronics, vol. 10, pp. 1363–1376, Sep. 2017. doi:10.1049/iet-pel.2016.0245

[13] H. Rezk, M. Aly, M. Al-Dhaifallah, and M. Shoyama, "Design and hardware implementation of new adaptive fuzzy logic-based MPPT control method for photovoltaic applications," IEEE Access, vol. 7, pp. 106427–106438, 2019. doi:10.1109/ACCESS.2019.2932694

[14] N. E. Zakzouk, A. K. Abdelsalam, A. A. Helal, and B. W. Williams, "PV single-phase grid-connected converter: DC-link voltage sensorless prospective," IEEE Journal of Emerging and Selected Topics in Power Electronics, vol. 5, no. 1, pp. 526–546, Mar. 2017. doi:10.1109/JESTPE.2016.2637000

[15] L. V. Bellinaso, H. H. Figueira, M. F. Basquera, R. P. Vieira, H. A. Gründling, and L. Michels, "Cascade control with adaptive voltage controller applied to photovoltaic boost converters," IEEE Transactions on Industry Applications, vol. 55, no. 2, pp. 1903–1912, Mar. 2019. doi:10.1109/TIA.2018.2884904

[16] R. Chinnappan, P. Logamani, and R. Ramasubbu, "Fixed frequency integral sliding-mode current-controlled MPPT boost converter for two-stage PV generation system," IET Circuits, Devices & Systems, vol. 13, no. 6, pp. 793–805, 2019. doi:10.1049/iet-cds.2018.5221

[17] R. Pradhan and B. Subudhi, "Double integral sliding mode MPPT control of a photovoltaic system," IEEE Transactions on Control Systems Technology, vol. 24, no. 1, pp. 285–292, Jan. 2016. doi:10.1109/TCST.2015.2420674

[18] P. Shaw, "Modelling and analysis of an analogue MPPT-based PV battery charging system utilising dc–dc boost converter," IET Renewable Power Generation, vol. 13, no. 11, pp. 1958–1967, May 2019. doi:10.1049/iet-rpg.2018.6273

[19] D. Espinoza-Trejo and J. Á. Pecina Sánchez, "Switch fault diagnosis for boost DC-DC converters in photovoltaic MPPT systems by using high-gain observers," IET Power Electronics, vol. 12, Jun. 2019. doi:10.1049/iet-pel.2018.6287

[20] A. Datta, R. Sarker, and I. Hazarika, "An efficient technique using modified p–q theory for controlling power flow in a single-stage single-phase grid-connected PV system," IEEE Transactions on Industrial Informatics, vol. 15, no. 8, pp. 4635–4645, Aug. 2019. doi:10.1109/TII.2018.2890197

[21] F. El Aamri, H. Maker, D. Sera, S. V. Spataru, J. M. Guerrero, and A. Mouhsen, "A direct maximum power point tracking method for single-phase grid-connected PV inverters," IEEE Transactions on Power Electronics, vol. 33, no. 10, pp. 8961–8971, Oct. 2018. doi:10.1109/TPEL.2017.2780858

[22] H. K. Khalil. Nonlinear Control. Pearson, pp. 263-280, 2015

[23] G. Farivar, B. Hredzak, and V. G. Agelidis, "A DC-side sensorless cascaded h-bridge multilevel converter-based photovoltaic system," IEEE Transactions on Industrial Electronics, vol. 63, no. 7, pp. 4233–4241, Jul. 2016. doi:10.1109/TIE.2016.2544243

[24] M. A. Elsaharty, H. A. Ashour, E. Rakhshani, E. Pouresmaeil, and J. P. S. Catalão, "A novel DC-bus sensor-less MPPT technique for single-stage PV grid-connected inverters," Energies, vol. 9, no. 4, Apr. 2016. doi:10.3390/en9040248

[25] G. Escobar, S. Pettersson, C. N. M. Ho, M. Karppanen, and T. Pulli, "PV current sensorless MPPT for a single-phase PV inverter," in IECON 2011 - 37th Annual Conference of the IEEE Industrial Electronics Society, Nov. 2011, pp. 3906–3911. doi:10.1109/IECON.2011.6119947

[26] R. Márquez, T. M. Guerra, M. Bernal, and A. Kruszewski, "A non-quadratic Lyapunov functional for H∞ control of nonlinear systems via Takagi–Sugeno models," Journal of the Franklin Institute, vol. 353, no. 4, pp. 781–796, Mar. 2016. doi:10.1016/j.jfranklin.2016.01.004

[27] T.-M. Guerra, M. Bernal, and M. Blandeau, "Reducing the number of vertices in some Takagi-Sugeno models: example in the mechanical field," IFAC-PapersOnLine, vol. 51, no. 10, pp. 133–138, Jan. 2018. doi:10.1016/j.ifacol.2018.06.250

[28] D. Quintana, V. Estrada-Manzo, and M. Bernal, "An exact handling of the gradient for overcoming persistent problems in nonlinear observer design via convex optimization techniques," Fuzzy Sets and Systems, vol. 416, pp. 125–140, Jul. 2021. doi:10.1016/j.fss.2020.04.012

[29] U. Vargas, A. Ramirez, and G. C. Lazaroiu, "Flexible extended harmonic domain approach for transient state analysis of switched systems," Electric Power Systems Research, vol. 155, pp. 40–47, Feb. 2018. doi:10.1016/j.epsr.2017.09.030

[30] Z. Lendek, T. M. Guerra, R. Babuška, and B. D. Schutter. Stability Analysis and Nonlinear Observer Design using Takagi-Sugeno Fuzzy Models. Berlin Heidelberg: Springer-Verlag, pp. 49-71, 2011. doi:10.1007/978-3-642-16776-8

[31] K. Ogata. Modern Control Engineering. Pearson, pp. 682-685, 2010

[32] R. A. D. J. Terán, J. Pérez, and J. A. Beristáin, "Tuning methodology for PI controllers in active power filters," DYNA Energía y Sostenibilidad, vol. 8, no. 1, pp. 11, Jan. 2019. doi:10.6036/ES9229

[33] B. Bendib, H. Belmili, and F. Krim, "A survey of the most used MPPT methods: Conventional and advanced algorithms applied for photovoltaic systems," Renewable and Sustainable Energy Reviews, vol. 45, pp. 637–648, May 2015. doi:10.1016/j.rser.2015.02.009

[34] Shabbir S. Bohra, "DC-current sensor-less MPPT based grid-fed single-phase photovoltaic (PV) micro-inverter," Appl. Sol. Energy, vol. 56, no. 2, pp. 85–93, Mar. 2020. doi:10.3103/S0003701X20020036

[35] H. Bahri, K. Oualifi, M. Aboulfatah, M. Guisser, O. S. Adekanle, and M. El Malah, "Nonlinear observer-based control for three phase grid connected photovoltaic system," in 2019 International Conference on Wireless Technologies, Embedded and Intelligent Systems (WITS), Apr. 2019. pp. 1–6. doi:10.1109/WITS.2019.8723685